WELDING RESEARCH

SUPPLEMENT TO THE *WELDING JOURNAL,* JANUARY 2002
Sponsored by the American Welding Society and the Welding Research Council

Development of Appropriate Resistance Spot Welding Practice for Transformation-Hardened Steels

A repeatable and effective methodology for producing a temper diagram for different steels is demonstrated

BY W. L. CHUKO AND J. E. GOULD

ABSTRACT. High-strength steels (HSS) are one of the most popular alternative materials for weight reduction in next-generation vehicles. One of the known concerns with using HSS is an issue called "hold-time sensitivity." Previous work has shown susceptibility to hold-time-related failures can be remedied through in-process quench and tempering of the weld.

In this study, dual-phase, transformation-hardened steels of 690- and 960-MPa (100- and 140-ksi) tensile strengths and nominally 0.9-mm (0.035-in.) gauge were examined. Each steel was welded and in-process quenched and tempered. A matrix of temper times and currents were used to define the range of effective tempering. Effectiveness of tempering was related to hardness of the weld nugget and corresponding temper diagrams were developed for each sample.

The resulting temper diagrams showed a characteristic C-curve shape for the main part of the diagram with a transient region that extended asymptotically to higher currents and shorter times. The C-shape supported the existence of steady-state thermal conditions for longer heating times during tempering. The transient region was associated with thermal mass effects at high currents and short temper times. Retransformation to austenite and subsequent quenching to martensite dictated the upper limit of the curve while lower currents and times characteristic of the initial transformation to martensite dictated the lower bound of the curve.

Chemistry and gauge of the material were the two critical factors influencing tempering response; processing did not appear to have a significant effect.

The goal of the study was to demonstrate a repeatable and effective methodology for producing a temper diagram for different steels. By documenting this methodology, temper diagrams could be used to define process requirements in order to increase the quality of spot welds in various types of transformation-hardened steels.

W. L. CHUKO (wayne_chuko@ewi.org) is Applications Engineer and J. E. GOULD is Principal Engineer in the Resistance and Solid State Welding Section, EWI Materials Joining Technology, Edison Welding Institute, Columbus, Ohio.

Introduction

The current pressure on automotive manufacturers to produce more fuel-efficient vehicles has shifted design trends to alternative lightweight materials. Some of these alternative materials include HSS, Al, Mg, plastics, and composite materials. All of these materials show strong potential as major construction materials for use in automobiles. Aluminum, in particular, has stirred a lot of interest in recent years (Refs. 1, 2), and an ongoing effort is being made toward furthering technical knowledge in this area. Cost, however, is still a restricting issue regarding Al, limiting its acceptance.

Historically, the majority of automobile structural components have been made of steel. Comfort levels with respect to performance and manufacturability of steel components is very high; therefore, many manufacturers would like to continue to use steel as the primary automobile structural material.

The evolution of steel technology has led to several different grades of HSS that offer certain advantages over typical low-carbon steels. High-strength steels offer greater specific strengths and, therefore, facilitate gauge reduction in the assembled component. This leads to an ultimate reduction in weight while increasing performance. Additionally, HSS are very cost competitive and formability is good.

High-strength steels have been used in automotive and other applications for some time. As early as the 1970s and '80s, extensive work was done regarding weldability with various types of HSS and application in the automotive industry (Ref. 3). With the current push toward lighter

KEY WORDS

High-Strength Steel
Automotive
Spot Welding
Hold Time
Temper Diagram
Transformation-Hardened

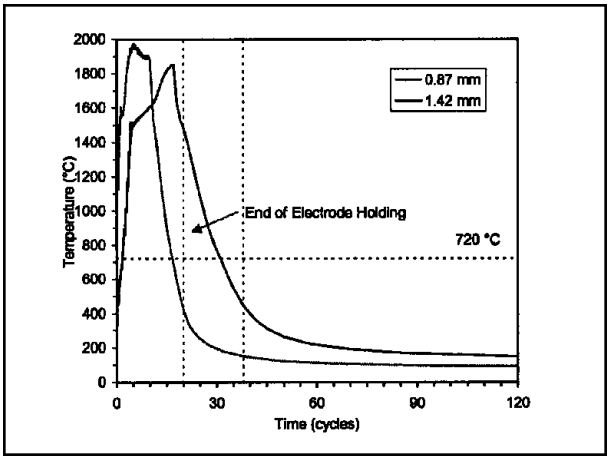

Fig. 1— Thermal modeling results show the cooling characteristics of resistance spot welds on 0.87- and 1.42-mm-thick material. (The 0.87-mm-thick material was modeled using 6.35-mm face diameter electrodes, for a weld time of 10 cycles. The 1.42-mm-thick material was modeled using 7.9-mm electrodes, for a weld time of 14 cycles.)

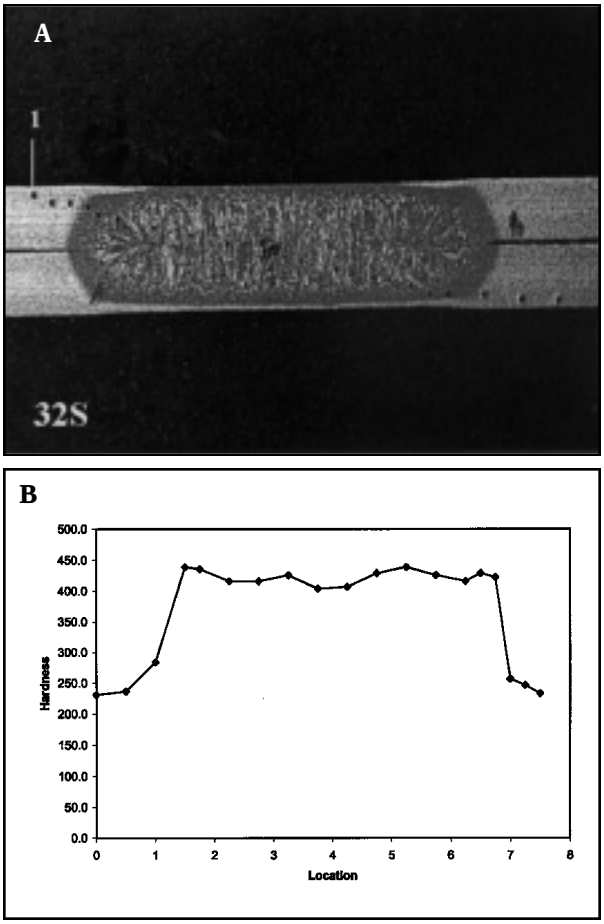

Fig. 2 — A — Weld nugget cross section; B — related hardness profile for an untempered resistance spot weld on 690-MPa (100-ksi) material.

automobiles, interest in HSS has been rekindled. High-strength steels achieve their strength through a combination of chemistry and processing, yielding tensile strengths ranging from 340 up to 1500 MPa (50 to 220 ksi). Newer HSS offer the potential of additional weight reduction due to gauge reduction.

This study focuses on the weldability of a specific class of HSS, namely transformation-hardened steels. These steels use varying fractions of degenerate martensite as a strengthening mechanism. Through complex thermal processing, strength levels up to 500 MPa (220 ksi) can be achieved. A specific welding-related concern regarding these steels is hold-time sensitivity, a phenomenon demonstrated during destructive (peel) testing. For typical hold times of 30 to 60 cycles, the spot weld fractures interfacially when peeled. For shorter hold times (5 cycles or less), however, the weld peels with a full button morphology. One proven method for remedying this from happening to hold-time-sensitive steels is in-process quench and tempering of the weld (Ref. 8). This method involves holding just-made weld between the electrodes long enough to sufficiently cool. A temper pulse is then applied to soften the microstructure of the weld. Steels of varying the composition and processing will react differently to tempering, and it is still unknown how some of the newer transformation-hardened steels will react during such tempering.

Background on High-Strength Steels

High-strength steels (HSS) generally fall into three basic categories classified by the strengthening mechanism employed. These include solid-solution-strengthened, grain-refined, and transformation-hardened steels. Manufacturing and material properties of the types of HSS are well documented in papers by Bleck (Ref. 3) and Davies and Magee (Ref. 4).

Transformation-hardened steels are the newest type of HSS being considered for use in the automotive industry. These steels use predominately higher levels of C and Mn along with heat treatment to increase strength. The finished product has a duplex microstructure of ferrite with varying levels of degenerate martensite. This allows for varying levels of strength. There are three basic types of transformation-hardened steels. These are dual-phase, transformation-induced plasticity (TRIP), and martensitic steels.

Dual-phase steels are annealed by first holding the strip in the $\alpha + \gamma$ temperature region for a set period of time. During the annealing time, C and Mn diffuse into the austenite leaving a ferrite of greater purity. The steel is then quenched so the austenite is transformed into martensite and the ferrite remains on cooling (Ref. 3). The strip is then subjected to a temper cycle to allow some level of martensite decomposition. By controlling the amount of martensite in the steel, as well as the degree of temper, the strength level can be controlled. Depending on processing and chemistry, the strength level can range from 350 to 960 MPa (50 to 140 ksi).

TRIP steels also use C and Mn, along with heat treatment, in order to retain small amounts of austenite and bainite in a ferrite matrix. These steels have a microstructure of metastable retained austenite in a predominately ferrite matrix along with small amounts of bainite (and other forms of decomposed austenite). This combination of microstructures has the added benefit of higher strengths in the range of 600 to 960 MPa (90 to 140 ksi) and resistance to necking during forming, which offers improved formability over other HSS (Ref. 3).

Martensitic steels, which have tensile strengths up to 1500 MPa (220 ksi), are fully quenched to martensite during processing. The martensite structure is then tempered back to the appropriate strength level, thus improving steel toughness.

Hold-Time Sensitivity

A steel is considered hold-time sensitive when, using conventional hold times of 30 to 60 cycles, the resulting weld shows interfacial failure and a full button morphology is observed when using reduced hold times (around 5 cycles or less). Indications of partial-button crack-

Table 1 — Strength Level, Gauge, and Composition of the Two Dual-Phase HSS Used in this Study

Tensile Strength MPa (ksi)	Gauge (mm)	Chemical Composition (%) C	Mn	P	S	Si
690 (100)	0.87	0.1422	1.3800	0.0080	0.0020	0.2860
960 (140)	0.87	0.1343	1.4000	0.0080	0.0020	0.2970

ing (so-called "irregular-buttons") are also indicative of hold-time sensitivity.

Causes for Hold-Time Sensitivity Failure

The occurrence of hold-time sensitivity is well documented (Refs. 5, 7, 8–13). However, the underlying causes have only recently been defined. Gould, Lehman, and Holmes (Ref. 6) suggested that susceptibility to interfacial failure was due to the following three factors: a disadvantageous stress state of the weld, the presence of preferential crack paths within the nugget, and a susceptible microstructure. Small nugget diameters combined with thicker sections resulted in a greater degree of triaxiality during peel testing. This disadvantageous stress state was known to promote interfacial failure. The presence of preferential crack paths, such as porosity or solidification cracks, could allow a crack to initiate at the faying surface notch and propagate from one porosity or crack location to another along the faying surface of the weld. Finally, a hardened microstructure with a large amount of martensite could result in brittle cleavage fracture.

That martensite can form in resistance spot welds, even at low carbon levels, is supported by the models of Gould, Li, Dong, and Kimchi (Ref. 7) and Feng, Gould, Babu, Santella, and Reimer (Ref. 14). These have shown that cooling rates associated with spot welding are extremely rapid, on the order of 10^3 to 10^5 °C/s. The hard martensite provides a path for a crack to propagate through. In addition, rapid cooling rates can lead to porosity entrapment toward the outer edges of the weld where the stress concentration is greatest in a peel test (Ref. 5). Rapid cooling rates have also been associated with a tendency for solidification cracking to occur, which can add to the chances of interfacial failure of a spot weld. Using shorter hold times can allow the weld to cool at a slower rate and, thus, minimize cracking. However, shorter hold times cannot be guaranteed by many industrial welding guns and are not always practical in automotive-assembly operations.

Chemistry of the particular steel is a major contributing factor to hold-time sensitivity. Additions of P, common in solid-solution-strengthened steels, have been associated with additional porosity in the solidified weld nugget (Ref. 5). As mentioned, the location and amount of porosity in a spot weld can affect its mode of failure in a peel test. Additions of C and Mn, the main elements that are added to transformation-hardened steels, are known to aid in the formation of martensite on cooling. These steels, of course, also have an increased risk of hold-time sensitivity.

Material thickness has multiple effects on the mode of failure during a peel test. First, the thickness of the material can alter the solidification mode. Thicker materials will allow for a slower, more three-dimensional mode of solidification. Slower cooling rates can reduce the tendency for solidification cracking. In addition, these slower cooling rates reduce the risk of martensitic formation. It has also been shown that slower cooling rates tend to relocate porosity away from the nugget periphery. As mentioned previously, however, thicker materials result in a greater degree of triaxiality on cooling.

Clearly, there are several factors contributing to hold-time sensitivity. Reasons for actual unacceptable weld failure are a combination of some, or all, of the factors involved.

Fracture Modes

Interfacial failure during a standard peel test in a HSS resistance spot weld is not uncommon. Research by Gould and Workman (Ref. 5), as well as Ferrasse, Verrier, and Messemaecker, et al. (Ref. 12), have shown that the cracking that occurs can be a combination of ductile and brittle fracture modes. Typically, the crack initiates at the faying surface notch between the sheets being joined. From there, it propagates through the weld nugget by following paths of hard brittle phases of martensite, or by following a path of porosity. Through either path, a combination of ductile and brittle cleavage-type fracture is seen. Work by Gould and Workman (Ref. 5) documented this on both solid-solution-strengthened and transformation-hardened steels.

Table 2 — Basic Welding Conditions Used for the Two Steels (0.87-mm Gauge) under Study

Welding Parameters	Steel 690 MPa (100 ksi)	960 MPa (140 ksi)
Expulsion Current (kA)	7.4	8.4
Force (N/lb)	3100/700	3100/700
Squeeze (cycles)	80	80
Weld (cycles)	10	10
Quench (cycles)	10	10
Temper (current + time)	Float	Float
Hold (cycles)	30	30

Experimental Procedure

Temper diagrams in this study were developed by applying the temper cycle directly in the welding program. Such temper cycles are now common on most programmable resistance welding control systems. On these controllers, tempering is simply added to the standard welding cycle by allowing a period of no current flow under full electrode force (quench time) followed by the application of the temper current (for a fixed temper time), and finally a hold time. In this way, resistance weld tempering can be accomplished without additional equipment or radically different cycle times.

The basic approach used for developing these temper diagrams was to take advantage of this capability, essentially coupling candidate temper cycles onto standard resistance spot welding schedules. Appropriate quench times were derived from thermal modeling data available in the literature. Temper currents were then varied from well below to above the apparent expulsion limit (for the appropriate steel) in a linear fashion, and temper times were varied in a geometrically progressing fashion. The magnitude of the tempering effect was then evaluated using hardness testing. The resulting temper diagram has been presented as a contour plot, showing the variation of hardnesses for all combinations of temper currents and times.

Materials and Equipment

Two materials were selected for evaluation in this study. These materials were chosen based on their potential for application in the automotive industry, availability, and tendency to exhibit hold-time sensitivity. These included 690- and 960-MPa (100- and 140-ksi) tensile strength steels, both of nominally 0.9-mm (0.035-in.) thickness. These are both classified as

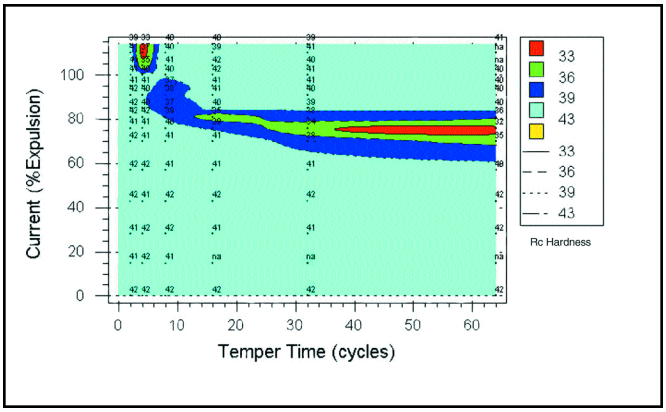

Fig. 3 — Temper diagram for resistance spot welds on the 690-MPa (100-ksi) steel. (Steel thickness was 0.87 mm. Welding practice included 6.35-mm electrodes, an expulsion current of 7.4 kA, 10 cycles of weld time, and a 10-cycle quench time.)

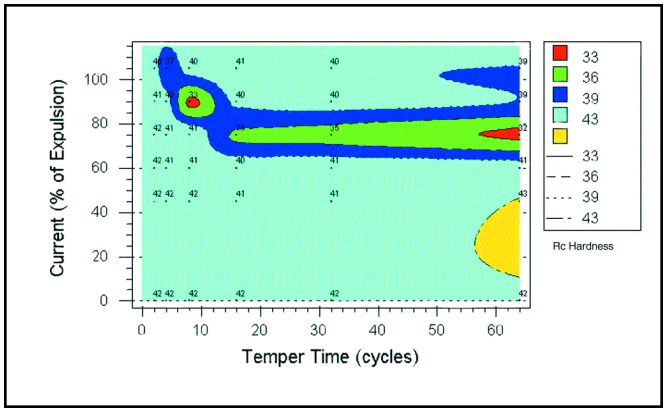

Fig. 4 — Temper diagram for resistance spot welds on the 960-MPa (140-ksi) steel. (Steel thickness was 0.87 mm. Welding practice included 6.35-mm electrodes, an expulsion current of 8.4 kA, 10 cycles of weld time, and a 10-cycle quench time.)

dual-phase steels. Exact gauges and compositions are provided in Table 1. This table suggests that the chemistries of these two steels are actually quite similar, with differences in strengths resulting from differences in heat treatment. The high C and Mn contents allowed verification of the temper diagram methodology described in this report.

Welding was done on a Taylor Winfield 30-kVA, single-phase AC, pedestal-type resistance spot welding machine equipped with an ATEK Tru-Amp controller. Welding was done using RWMA Class II copper electrodes, with a 6.35-mm (0.25-in.) face diameter and a 45-deg, truncated cone geometry. Electrodes were water cooled with a flow rate of 4.75 L/min (1.25 gal/min).

Welding Parameters

Base welding schedules were selected nominally following Ford Motor Company specification BA 13-4 (Ref. 17). To identify the necessary process limits for developing the temper diagram, a current range on each material was first conducted. This was done nominally to establish the expulsion current for each material. Resulting welding process conditions are presented in Table 2.

Temper Diagram Procedure Development

A matrix of temper times and currents were used to define the range of effective tempering. Effectiveness of tempering was related to hardness of the weld nugget and the corresponding temper diagrams were formed for each sample. The goal of the study was then to demonstrate a repeatable and effective methodology for producing a temper diagram for different steels. By documenting this methodology, temper diagrams could be used to define process requirements in order to increase the quality of spot welds on various types of transformation-hardened steels.

All welding was done on specially prepared 50 x 100-mm (2 x 4-in.) coupons (Ref. 17) used for 960-MPa (140-ksi) tensile strength steel, while 25 x 100-mm (1 x 4-in.) coupons were used for 690-MPa (100-ksi) tensile strength steel. In this latter case, smaller coupons were used due to a lack of material. Temper diagrams were then developed in the following steps:

1) Current-range evaluations. Steels were first subjected to current range testing per Ford Specification BA 13-4 (Ref. 17). This was done largely to establish the base (expulsion) current for the temper diagram development.

2) Quench time selection. Quench time was then selected. This was done using available thermal modeling and previous experience. For this gauge of steels, a quench time of 10 cycles was selected.

3) Welding trials. Welds were then made over a range of tempering currents and times. Welds were configured as standard peel test coupons, including both a shunt weld and a test weld. This approach is used in order to better simulate autobody construction, where shunt welds are always present. All subsequent evaluations were done on the test weld of the coupon.

4) Initial temper diagram matrix. A coarse approximation of the temper characteristics of each material was made using a linear variation of the temper current and a geometric progression of welding currents. Temper currents began at 15% of the expulsion current established during current range testing. The temper current was then increased by increments of 15% of the expulsion current up to 120% of the expulsion current (15, 30, 45, 60, 75, 90, 105, and 120% of the welding current). Tempering times began at 2 cycles and progressively doubled to a maximum of 64 cycles (2, 4, 8, 16, 32, and 64 cycles).

5) Hardness testing. One surface of each sample was then ground flat for hardness testing. On each sample, a single Rockwell C (R_c) hardness test was performed in the center of the weld surface. These hardness tests correlated well with microhardness tests taken across sectioned welds. The surface hardness measurements were used for subsequent contour plots.

6) Preliminary contour plotting. Rockwell C hardness values were then plotted in a two-dimensional contour plot as a function of temper current and time. This preliminary contour plot allowed critical areas of the diagram (where hardness changed most radically as a function of temper currents and times) to be identified.

7) Diagram refinement trials. Based on the results of the preliminary contour plot, additional temper trials were made. These trials were used largely to refine the "nose" of the temper curve and were made at much finer increments of current and time. Resulting welds were prepared and hardness tested in the fashion described in Step (5) above.

8) Preparation of final temper diagrams. Temper diagrams were then prepared using a MINITAB contour-plotting package. This package allowed some averaging of the data, as scatter is inherent with most hardness testing. Final temper diagrams took advantage of the results from both preliminary and refinement tempering trials.

Hardness Testing and Metallographic Support

As suggested above, both macro- and microhardness testing were performed. Macro surface hardness testing was performed using the standard R_c method, with a 150-kg load and a 120-deg pyramid indenter. Microhardness testing was done using Vickers' methods with a 1-kg load and a diamond pyramid indenter. Metallographic sectioning and polishing was done using standard techniques. Representative welds were then etched in Nital and examined using standard metallographic techniques.

Results

Estimations of Required Quench Times

As mentioned above, quench time, which is the time elapsed between completion of welding and application of the tempering current, was largely estimated from thermal modeling results. In this case, the model previously published by Li, Dong, and Kimchi (Ref. 7) was used. The resulting heating and cooling profile for a resistance spot weld made on 0.87-mm-thick (0.035-in.) steel using 6.35-mm (0.25-in.) face diameter electrodes, 8-kA welding current, and a 10-cycle weld time is presented in Fig. 1. These results suggest a cooling rate for this weld configuration on the order of 9000°C/s (16,200°F/s). This corresponds to a temperature of roughly 400°C (752°F) after a quench time of 10 cycles. For this material, a martensite finish (M_s) temperature of roughly 720°C (1328°F) can be calculated. The M_f temperature was established by using the M_s temperature calculated by Babu (Ref. 20). Then, based on the calculation of Koistien and Marburge (Ref. 21), a roughly 220°C temperature drop was calculated to form 90% martensite. This results in an M_f temperature of roughly 500°C. Based on these calculated values, using a 10-cycle quench time allows the spot weld to cool roughly 100°C (212°F) below the M_f temperature, facilitating transformation to martensite. This roughly 100°C supercooling should also be sufficient to take into account any change in the M_f temperature due to grain size or local compositional effects. This quench time, then, offers the best compromise between full quenching, minimum quench time, and maintaining residual heat in the weld. This residual heat is important, as less current is then required for the subsequent temper cycle. Based on these results, the 10-cycle quench time was used for all weld trials in this study. Note, however, that this minimum required quench time is strongly a function of material thickness. Also shown in Fig. 1 is a thermal profile for a resistance spot weld made on slightly thicker [1.42-mm (0.056-in.)] steel. Larger electrodes [7.9-mm (0.31-in.)], longer weld times (14 cycles), and higher currents (9-kA) are required for this steel. It can be seen from this plot that cooling rates for this thicker material are substantially reduced (4000°C/s). This suggests that roughly double the cooling time (20 cycles) would be required to achieve quenching to below the M_f temperature on this thicker material.

Surface Macrohardness/Microhardness Comparisons

To simplify the procedure for creating these temper diagrams, macrohardness measurements were made on the surface of all specimens. This eliminated both the need for sectioning and polishing specimens and the need to make full hardness traces. The R_c measurements also used a reasonably larger indenting tool, so influences of surface and small variations in microstructure were minimized. R_c measurements should also be accurate on these welds; the final joint thickness [1.5 to 1.8 mm (0.060 to 0.070 in.)] was thicker than the minimum sample thickness for R_c testing in the hardness ranges observed [roughly 1.4 mm (0.050 in.)] (Ref. 19). However, potential variations in through-thickness microstructure, as well as sample compliance concerns, necessitated verification of these surface hardness readings with microhardness results.

Such microhardness results for a representative untempered weld on the 690-MPa (100-ksi) steel are presented in Fig. 2. Included in this plot is a macrograph of the weld and the corresponding microhardness profile. The microhardness profile is relatively typical for higher carbon steel resistance spot welds. This consists of a relatively flat hardness profile across the weld itself, with the hardness dropping through the heat-affected zone (HAZ) to the base metal level. The hardness in the weld zone with this type of profile typically represents the hardness of martensite for the particular steel. For this weld, that hardness is roughly 450 VHN, which roughly corresponds to a 45 R_c hardness. Surface hardness measurements of similar welds show a hardness of R_c 42, demonstrating the accuracy of the surface measurement technique. That the surface hardness measurement is relatively low (R_c 42 vs. 45), however, suggests microstructural variations at the electrode sheet surface and sample compliance play at least a minor role. However, the technique is certainly accurate enough to characterize trends in tempering behavior in these spot welds.

Temper Diagrams for the 690- and 960-MPa (100- and 140-ksi) HSS

The resulting temper diagram for the 690-MPa (100-ksi) steel is presented in Fig. 3. Peak hardness on this diagram is in the range of R_c 42, and is typical of martensite for this hardenability of steel. Hardnesses on this diagram ranged from this high of R_c 42, down to a low level of R_c 32. The tempering curve is largely defined by the C curve, with peak tempering response around 78% of the expulsion current. For this region of the curve, effective softening of the martensite begins around 10 cycles of weld time, with peak softening occurring after about 35 cycles of temper time. The range of temper currents in this region of the diagram was relatively narrow, with softening occurring only between roughly 62 and 82% of the expulsion current.

This temper curve also contained a second component, however, sloping toward higher currents and shorter times in an asymptotic fashion. In this region of the curve, effective tempering was seen at currents as high as 120% of the expulsion current. However, the window of the curve in this region was relatively small, with variations of 3% heat or 5 cycles of weld time, effectively eliminating the tempering effect.

The temper diagram for the 960-MPa (140-ksi) HSS is presented in Fig. 4. Within experimental error, this diagram is virtually identical to that generated for the 690-MPa (100-ksi) steel. The nose of the C curve is again generally bounded between 62 and 82% of the expulsion current, with first softening (within the nose) occurring at 10 cycles and peak softening occurring at around 30–35 cycles. The curve also shows asymptotic upward drift toward higher currents and shorter tempering times. The ranges of currents and times of effective softening for this region of the curve were again relatively narrow.

Discussion

General Characteristics of Temper Diagrams

As described above, these temper diagrams generally consist of two distinct regions, a C-curve-shaped region, characteristic of isothermal transformation behavior, and a transient region at shorter times and higher currents. That the C-curve-shaped region of the curve resembles an isothermal transformation diagram is not surprising. For extended heating times, resistance heating during resistance spot welding essentially becomes balanced with heat extraction via thermal conduction through the electrodes. This effect has been reported pre-

viously (Ref. 18). Once this occurs, the temperature distribution within the resistance spot weld essentially becomes static. This, of course, defines an isothermal condition and accounts for the general shape of the C-curve region of the temper diagram. For this region of the diagrams, tempering currents above 82% of the expulsion current apparently cause the structure to retransform to austenite; once this current is terminated, this austenite quickly quenches to martensite. The lower boundary of this C curve is defined by the locus of temperature and time (current and time) required to initiate martensite decomposition. As diffusivities typically decrease exponentially with temperature, small decreases in current require ever-longer temper times for the tempering effect to be observed. It is of interest here that the slopes on the bottoms of these C curves are relatively flat, suggesting the range of tempering times used (2–60 cycles) are relatively short compared to the overall tempering response of martensite in these steels.

The tempering diagrams presented here deviate from typical isothermal tempering diagrams by the presence of the transient region at shorter temper times and higher temper currents. This region of the curve is believed to be due to the latent heat effects associated with heating the sample (under the applied current) from quench temperature to tempering temperature. For short temper times, steady-state conditions are not achieved, so currents no longer can be directly correlated with the temperature in the weld. Shorter times at higher currents, effectively then, represent an isothermal extension of the C curve to shorter times. For conventional isothermal diagrams, it is generally assumed these transient effects occur over a negligible period of time (compared to the events represented by the curve) and need not be considered. Here, however, it is clear these effects extend to as much as 30% of the tempering times studied and cannot be neglected.

Also note the particular quench time used for generating these curves. As mentioned above, this quench time correlated to a minimum value necessary to fully transform the structure to martensite and facilitated overall minimum-duration temper cycles. However, since these welds were not fully cooled (to the cooling water temperature), some residual heat remained in the weld at the initiation of the temper current. Such latent heat implies less heating was required to achieve specific tempering temperatures. In addition, the workpiece stack-up resistance was higher, increasing heat generation for a specific current. Clearly, the relative position of the temper diagram (with respect to currents and times) will change for different quench times (perhaps in a drastic way) and needs to be considered in further diagram development.

Steel-Related Effects on Temper Diagrams

Dual-phase HSS use a specific combination of steel chemistry and thermal processing to achieve the desired combinations of strength and ductility characteristic of these materials. With respect to these temper diagrams, however, base steel chemistry is the dominant characteristic of concern. This is because the bulk of the weld microstructure was transformed to austenite on heating and quenched, presumably, to martensite on cooling. In this process, any structure from the applied thermal processing was destroyed and the residual carbon variations (related to separate ferrite and degenerate martensite grains) were homogenized. Therefore, subsequent austenite decomposition was largely a function of the steel composition and cooling rate. Conversely, tempering response was a function of composition, mode of austenite decomposition, and applied temper cycle.

With respect to chemistry, hardenability additions (C, Mn, Si) have a dominant effect. In typical dual-phase steels, C, Mn, and Si additions all suppress the A_3 (ferrite + austenite ↔ austenite phase boundary) temperature, as well as slow the kinetics of the subsequent martensite decomposition during tempering. More heavily alloyed steels, then, can be expected to show tempering curves displaced to lower current levels and require longer tempering times.

Gauge, of course, should also play a major role in the shape and location of these diagrams. Most notably, as described above, heavier gauge steels act as larger thermal masses during resistance spot welding. In addition, increases in steel thickness restrict heat flow away from the weld into the electrodes (Ref. 18). This has a number of effects, including (as noted) mandating longer quench times to form martensite, as well as longer heating times to reach steady-state temperatures in the weld during tempering. These effects should essentially shift the temper curve to longer times, and potentially lower relative currents (as a percent of expulsion) for heavier gauge steels.

It was of note that the temper diagrams for these two steels were quite similar. This was because the steels were of a similar gauge and a similar composition with differences in the specified strength level being largely determined by thermal processing. Based on the above discussions, steels of similar composition and gauge, welded with similar practice, should yield similar temper diagrams. The results presented here suggest they do.

Applying Temper Cycles to Production Welding

These curves do indicate that for the higher C and Mn HSS, temper cycles can be used to substantially reduce weld hardness and, presumably, hold-time sensitivity. These curves, however, can be applied in a number of different ways. In applying these curves, quench time is the first factor to be considered. Ideally, sufficient quench times should be allowed to permit the weld to achieve stable, sub-M_f temperature. Clearly, the most robust approach would be to cool the weld to the temperature of the electrode cooling water. If shorter cycle times are needed, however, minimum quench times to complete the martensite transformation may be used. As pointed out above, these temper curves can potentially vary with quench time, so the right temper diagram must be used.

With respect to tempering currents and tempering times, the most robust applications of these diagrams use temper currents defined by the nose of the base C curve, with a temper time on the order of 30–35 cycles. This provides a maximum of tempering (within a reasonable time), with a temper schedule that is robust to both temper current and temper time variations. Where shorter cycle times are required, these diagrams suggest potential for very short, high-current temper cycles to be used. These temper times apparently can be as short as 5–10 cycles. However, tempering under these conditions is not very robust, and actual weld hardnesses may vary under production conditions.

Conclusions

In this study, the concept of a diagram defining postweld in-situ tempering (postweld tempering incorporated in the welding cycle) behavior of resistance spot welds on C-Mn grades of HSS has been introduced. This diagram is based on the fact C-Mn sheet steels typically transform to martensite on cooling during resistance spot welding. Tempering can then be accomplished by adding a tempering step (temper current, temper time) to the welding sequence. This tempering step is a relatively simple way of reducing weld hardnesses and, therefore, susceptibility to hold-time sensitivity behavior. The methodology for producing these tempering diagrams was developed and diagrams were produced for some represen-

tative C/Mn-type HSS. The diagrams were then interpreted based on the underlying steel metallurgy, as well as the thermal cycles implicit in the tempering operation itself. Specific conclusions include the following:

- The methodology, based on varying the temper current linearly, and the temper time in a geometric progression was an effective method for producing resistance spot welding temper diagrams.
- Rockwell C hardness testing on the outer surface of the spot weld was an efficient method of evaluating weld hardness. These results correlated with hardness traverses across representative joints.
- The methodology for developing temper diagrams resulted in similar diagrams for both the 690- and 960-MPa (100 to 140-ksi) dual-phase steels. Both diagrams resulted in a characteristic C-curve shape, although this basic curve extended asymptotically to higher currents and shorter times.
- The main part of the temper diagram was a typical isothermal transformation C curve. This confirmed that for longer heating times, steady-state thermal conditions exist in resistance spot welds.
- The isothermal region of the temper diagram was bounded by an upper and lower limit of temper currents and times. Retransformation to austenite and subsequent quenching to martensite explains the upper bound of the curve and lower temper currents and times characteristic of initial martensite decomposition explain the lower bound of the curve.
- This transient region of the temper diagram was associated with thermal mass effects and the temperature rise characteristics associated with short heat times. For these shorter times, higher currents were required to achieve temperatures where martensite decomposition could occur.
- Temper response was based only on the composition and gauge of the steel under consideration. Since the two steels studied were of similar gauge and composition, nearly identical tempering response was observed.
- The best application of in-process tempering can be applied to production welding practice by using lower currents and longer (30–35 cycles) tempering times. This provides the most robust tempering response. High-current, short-time tempering can be done, but actual weld hardnesses may vary under production conditions.

References

1. Kurihara, Y. 1993. The role of aluminum in automotive weight reduction, part 1. J. of Metals 45(11): 32–33.

2. Tuler, F., Warren, A., Mariano, S., and Wheeler, M. 1994. Overall benefits and value of aluminum for an automobile body structure. IBEC94 Proceedings, Automotive Body Materials, pp. 8–14, IBEC Ltd., Warren, Mich.

3. Bleck, W. 1996. Cold-rolled, high-strength sheet steels for auto applications. J. of Metals (7): 26–30.

4. Davies, R. G., and Magee, C. L. 1979. Physical metallurgy of automotive high strength steels, structure and properties of dual-phase steels. AIME Annual Meeting, New Orleans, La.

5. Gould, J. E., and Workman, D. 1998. Fracture morphologies of resistance spot welds exhibiting hold time sensitivity. Proceedings of Sheet Metal Welding Conference VIII, AWS Detroit Section, Detroit, Mich.

6. Gould, J. E., Lehman, L. R., and Holmes, S. 1996. A design-of-experiments evaluation of factors affecting the resistance spot weldability of high-strength steels. Proceedings of Sheet Metal Welding Conference VII, AWS Detroit Section, Detroit, Mich.

7. Li, M. V., Dong, P., and Kimchi, M. 1997. Modeling and analysis of microstructure development in resistance spot welds of high strength steels. 98IBECC-8.

8. Dickinson, D. W. 1981. Welding in the Automotive Industry. Republic Steel Research Report SG 81-5.

9. Gould, J. E. 1994. Modeling primary dendrite arm spacings in resistance spot welds, part 1 — modeling studies. Welding Journal 73(4): 67-s to 74-s.

10. Gould, J. E. 1994. Modeling primary dendrite arm spacings in resistance spot welds, part 2 — experimental studies. Welding Journal 73(5): 91-s to 100-s.

11. Peterson, W. 1997. Dilution of weld metal to eliminate interfacial fractures of spot welds in high and ultra high strength steels. ICAWT, Columbus, Ohio.

12. Ferrasse, S., Verrier, P., and Meesemaecker, F. 1998. Resistance spot weldability of high strength steels for use in car industry. Welding in the World.

13. Han, Z., Indacochea, J. E., Chen, C. H., and Bhat, S. 1993. Weld nugget development and integrity in resistance spot welding of high-strength cold-rolled sheet steels. Welding Journal 72(7): 209-s to 216-s.

14. Feng, Z., Gould, J. E., Babu, S. S., Santella, M. L., and Reimer, B. W. Model for resistance spot welding. Department of Energy.

15. Metals Handbook. 1948. pp. 494–502, ASM International, Materials Park, Ohio.

16. Linnert, G. E. 1994. Welding Metallurgy, Vol. 1, pp. 157–161.

17. Ford Motor Company. 1980. Resistance spot weldability tests for high strength steels. Ford Laboratory Test Methods, BA 13-4.

18. Gould, J. E. 1987. Experimental and analytical studies of nugget development during resistance spot welding. Welding Journal 66(1):1-s to 10-s.

19. Metals Handbook. 1948. ASM international, Materials Park, Ohio.

20. Oak Ridge National Laboratory Website,http://engm01.ms.ornl.gov/IGORgraph1acgi.

21. Koistien, D. P., and Marburge, R. E. 1959. A general equation prescribing the extent of the austenite-martensite transformation in pure iron-carbon alloys and plain carbon steels. Acta Metallurgica 7: 59–60.